Using Perovskite Nanoparticles as Halide Reservoirs in Catalysis and as Spectrochemical Probes of Ions in Solution

Tennyson L. Doane[1]*, Kayla L. Ryan[1], Laxmikant Pathade[1], Kevin J. Cruz[1],

Huidong Zang[2], Mircea Cotlet[2], Mathew M. Maye[1]*

[1]Department of Chemistry, Syracuse University, Syracuse NY, 13244

[2]Center for Functional Nanomaterials, Brookhaven National Laboratory, Upton NY, 11973

**tdoane@syr.edu* and **mmmaye@syr.edu*

SUPPORTING INFORMATION

Chemicals and Instrumentation

Lead iodide (99%), lead bromide (99.99%), lead chloride (99.99%) cesium carbonate (97%), oleylamine (70%, technical grade), oleic acid (90%), octadecene (90%), tetraoctylammonium bromide (98%), tetraoctylammonium chloride (97%), silver nitrate (99%), octylamine (99%), 1-butanol (anhydrous, 99.8%), 1-butyl, 3-methylimidazolium tetrafluoroborate (97%), zinc perchlorate hexahydrate and methylphosphonic acid (98%) were purchased from Sigma Aldrich. Hexylphosphonic acid (HPA, 95%) and octylphosphonic acid (OPA, 97%) were purchased from STREM Chemicals. Tetraoctylammonium iodide (98%) was purchased from TCI, lead acetate (ACS grade) was used from Baker Analytics, reagent grade hexane and acetone was purchased from BDH, and 200 proof ethanol from Pharmco-AAPER. Tetrabutylammonium fluoride, 2-bromododecanoic acid, sodium tetrafluoroborate and lauric acid were graciously donated. Benzene-d6 (99.6%) and methanol-d4 (99.8%) were from Cambridge Isotope Laboratories. *Cis*-2-decenoic acid was purchased from Adipogen. All chemicals were used without further purification.

UV-Vis spectra were measured with a Cary100-Bio equipped with a temperature controller, and PL spectra and kinetics were measured using a Horiba Jobin Yvon Fluoromax-4 fluorimeter with typical slit settings of 2 and excitation at 400 nm. Colorimetric assay calibration was conducted with a Cary Eclipse Fluorimeter while kinetic measurements were running simultaneously. Quantum yields were measured versus rhodamine 6G in ethanol (QY = 0.95).[1] Digital images were taken with a Cannon Rebel EOS T5. A glass 96-well plate (Zinnser) was used for the colorimetric conversions shown in Fig. 4. NMR spectra were recorded with a Bruker Avance III HD 400 MHz NMR spectrometer using a sweep width of 15 ppm. A Bruker AXS D8 ADVANCE powder X-ray diffractometer was used for investigating $CsPbX_3$ nanoparticle (P-NP) lattice structure.

Purification of $CsPbX_3$ P-NPs

The as-synthesized P-NPs were diluted in excess hexane (1 mL of P-NP solution to 20 mL of hexane) under inert atmosphere to ensure stability. We find that the transition of cubic $CsPbI_3$ to the PL inactive yellow phase is accelerated in air and at high P-NP concentrations. Particles were stored under Ar and in a desiccator to ensure long stability. Additionally, keeping the solutions at 4°C also prolonged their viability. Adding excess oleic acid and oleylamine led to eventual dissolution of the particles evidenced by increasingly fainter color and PL intensity (data not shown). $CsPbX_3$ P-NPs were cleaned by centrifuging 1 mL of the diluted solution at 5000 rpm (1884xg) for 1 min in a fixed angle bench top centrifuge; the supernatant was transferred to a new EP tube, concentrated under an Ar stream, and diluted to 1.5 mL with 1-butanol or ethyl acetate. The mixture was centrifuged at 10,000 rpm (7378xg) for 1 min, and after discarding the supernatant the precipitated NPs were re-dissolved in hexane. Alternatively, 1 mL of the reaction mixture could be injected into 20 mL of 1-butanol to clean the particles directly via sedimentation. The supernatant was removed leaving behind clean $CsPbX_3$ P-NPs, which could be re-suspended in hexane. Estimated concentration of P-NPs was calculated based on serial dilution of the stock solution assuming near unity yields and minimal loss during cleaning, and therefore the concentrations should be taken as an upper limit.

Synthesis of Tetraoctylammonium and Cesium Halide-Alternative Salts

The generation of non-halide tetraoctylammonium (TOA^+) and cesium salts was completed using a precipitation method. A 0.1 M solution of the desired anion salt ($AgNO_3$, $Pd(CH_3COO)_2$, and $Zn(ClO_4)_2$) was prepared in the presence of a slight excess (~10%) of either TOA^+-halide or $Cs_2(CO_3)$, and mixed in methanol to precipitate out the metal ion (AgBr/AgI, PbBr, and $ZnCO_3$). The solution was centrifuged for 1 min at 7378×g to collect the insoluble precipitate, and the supernatant was transferred to a clean centrifuge tube. The methanol was evaporated slowly under an Ar stream and then the oily residue was re-suspended with 1-butanol and used without further purification. The precipitation efficiency can be estimated based on the solubility products, k_{sp} as follows: $PbBr_2$ (6.6×10^{-6}) < PbI_2 (9.8×10^{-9}) < $ZnCO_3$ (1.46×10^{-10}) < AgBr (5.35×10^{-13}) < AgI (8.52×10^{-17}),[2] so that both the acetate and perchlorate salts likely have poorer yields than the corresponding nitrates. Furthermore, the solubility of $CsClO_4$ will be much poorer than the alkylammonium nitrates, so that the concentrations reported for the indicator shown in Figure 8 should be taken as approximate only.

Tetraoctylammnoium tetrafluoroborate ($TOABF_4$) was prepared using a variation of a previously established method.[3] Briefly, 328 mg of tetraoctylammonium iodide (0.55 mmols) was dissolved in 5 mL of CH_2Cl_2 and mixed with 5mL of an aqueous 0.258M $NaBF_4$ solution (1.29 mmols) with vigorous stirring for 48 hours. The resulting product was extracted 3 times with water, dried over $MgSO_4$, and then rotovapped to a dry powder. The final yield was 63 mg (21% yield) which was dissolved in 10 mL of 1-butanol to give a 23 mM $TOABF_4$ solution, although this solution seemed saturated. No obvious precipitation was observed in the presence of 0.2M lead acetate or 0.08M silver nitrate solutions in ethanol ensuring low halide content. We observed that tetrabutylammonium salts (TBAX) had poor solubility in non-polar solvents, requiring the use of TOA^+ salts or excess P-NP ligands to ensure smooth ion exchange.

NMR Measurements of Reaction Products

The reaction of 2-bromododecanoic acid and octylamine was monitored in deuterated benzene (C_6D_6), and the effect of carboxylic acid dissociation on chemical shifts was confirmed in CD_3OD (Fig. S12). Briefly, 2 mM 2-bromolauric acid and octylamine (equimolar concentrations) were reacted in C_6D_6 in the presence of P-NPs (~20 μg) to induce a Finkelstein reaction. The NMR data was taken at time 0, after 60 minutes in a 50°C water bath, and in 24 hour increments up to 96 hours at room temperature. The color change observed in Figure 5c was also monitored via PL measurements, with a final emission wavelength of 517 nm. Similarly, a sample of 2-Br and OA in C_6D_6 was also prepared at a 1:1 ratio (~11 mM) and this was subjected to the same sampling conditions as the P-NP reaction mixture.

Attempts to identify the Finkelstein product via NMR were done using 20 mL of a dilute solution of $CsPbI_3$ P-NPs (~200 μ g) with 0.1 mM 2-bromododecanoic acid and octylamine (equimolar concentrations) in hexane, which was allowed to react for ~4 days until the emission was green under UV-irradiation. The solution was purified *via* a silica column, and the resulting filtrate (which had no emission under UV irradiation) was rotary evaporated, and resuspended in C_6D_6. The resulting NMR spectrum was heavily saturated with signatures from original particle solution (Figure S14a) but shifts in the 4-5 ppm region were used to identify 2-iododododecanoic acid (2-I, Figure S14b). To identify the NMR signatures associated with 2-I, 2-Br was reacted with two-fold excess of tetraoctylammonium iodide in hexane with mild heating (water bath, ~35°C) for 15 minutes. A marked color change was observed, and subsequent rotary evaporation resulted in a yellow oil, with a new NMR signature at ~ 4.39 ppm (Figure S14b).

XRD Sample Preparation

Samples of $CsPbX_3$ NPs were cleaned and prepared for XRD under an inert atmosphere by drop-wise addition of a concentrated sample onto an XRD grid. The samples were then transported under Ar to the XRD chamber and placed under vacuum. Conversion of $CsPbI_3$ to $CsPbI_{3-x}(NO_3)_x$ and $CsPbI_{3-x}(BF_4)_x$ was undertaken by mixing the P-NPs with 2 and 6 μmols of the anion, respectively, and subsequently concentrated for measurement.

Calculation of the Goldschmidt Tolerance Factor

The Goldschmidt tolerance factor is an indicator in ABX_3 perovskite crystal structure, which generally must lie between 0.81 and 1.1 for stable halide perovskites.[4] The tolerance factor is based on the size of the cations (A and B) and that of the anions, according to the equation:[4]

$$t = \frac{r_a + r_x}{\sqrt{2}(r_b + r_x)} \qquad \text{(Eq. 1)}$$

where r_a is the monovalent cation ionic radius, r_b is the divalent cation radius, and r_x is the monovalent anion radius. To calculate the tolerance factor, we have used the ionic radii for the cations and the thermochemical ionic radii for the anions,[5] which allows for an estimation of the space occupied by non-spherical molecules (i.e. nitrate, acetate, perchlorates, and

tetrafluoroborates). Figure S15a shows the calculated tolerance factors for the variety of anions explored in this work.

An additional parameter which has been correlated to perovskite formability is the so called octahedral factor, μ, which can be defined as:[6]

$$\mu = r_b/r_x \quad \text{(Eq. 2)}$$

which when plotted against t creates a formability map, where points which lie in the range of t = 0.81-1.11 and μ = 0.44-0.90 are considered stable. Figure S15b shows that all of the perovskites based on the anions investigated fall within this range.

The exact values of T and μ are dependent on what radii is used (ionic, crystal lattice, or thermochemical) but for consistency with the literature[6] we have used the 1.19Å for Pb^{+2} and 1.88Å for Cs^{+2},[7] but only the calculated thermochemical ionic radii for all of the anions[5] for estimating non-spherical anion compositions (tetrafluoroborate, nitrate, etc.) which results in some slight deviations.

Role of Halide Concentration and Solvent Influence on Conversion Efficiency

The specific parameters necessary for converting a $CsPbX_3$ P-NP focus on three main criteria: amount of halide available for substitution, solvation dynamics, and the ligand to particle ratio in solution. Figure S9a and b shows the effect of initial Br- concentration on the final optical properties. When the initial Br- concentration is low, the final PL intensity is vanishingly small (~5% PL retention), whereas "saturating" the solution with sufficient Br- leads to excellent conversion (~80% retention), even if the wavelengths of emission are similar. We have observed that when we titrate the NPs incrementally with TOABr, two different populations emerge with PL max that reflects the increasing Br concentration and another which is more shifted to the original emission wavelength (data not shown). In all cases, slow titration led to a decreased overall PL. In contrast, supplying the solution immediately with sufficient halide and/or placing the solution under strong convection led to a much better PL yield. We speculate that the rate at which halide equilibrium throughout the solution is reached is largely responsible for this process, and that both internal traps due to defects and ligand coverage as a function of exchange time lead to poorer optical yields.

The halide and ligand equilibrium hypothesis is supported by another observation we have made involving solvation dynamics and ligand-particle ratios. We have observed (Figure S9c and d) that PL retention in pure hexane are poorer than in a mixture of 50:50 hexane/1-butanol (Figure S9a and b) when converting $CsPbI_3$ to $CsPbBr_3$ with TOABr, even though the same total concentration of Br^- was being added in both cases. Moreover, when we tried to wash converted particles with mixed Br/I composition (yellow emission), we found that 1-butanol led to red emission ($CsPbI_3$) products while washing with ethyl acetate led to green ($CsPbBr_3$) emission (Figure S8). This suggests that the dissociation of alkylammonium halide salts as a function of chemical environment also plays an important role; we would expect the "harder" Br^- atom to dissociate better in 1-butanol (leading to competitive I^- incorporation) and the less polar I^- to have better solubility in non-polar media (leading to Br^- incorporation). These observations

reinforce the idea that these NPs should be regarded as being in a dynamic equilibrium with their surroundings rather than inert nanomaterials.

Prediction of Relative Oxidation Strength in Organic Solvents

The poor stability of $CsPbI_3$ is well known in the literature, especially to both water hydrolysis and oxygen based oxidation.[8] This is largely due to the low oxidation potential of iodide ions to iodine or triodide, which in aqueous solution proceeds as:

$$2I^- \rightarrow I_2 + 2e^- \qquad -0.5355\ V \qquad \text{(Eq. 3)}$$

$$3I^- \rightarrow I_3^- + 2e^- \qquad -0.536\ V \qquad \text{(Eq. 4)}$$

The corresponding 2 electron reactions for Br^-, Cl^-, and F^- ions, however, have significantly higher oxidation potentials of -1.066 V, -1.358 V, and -2.866 V, respectively.[2] The differences in oxidation potentials coupled with the inherent photoluminescent behavior of the NP opens the possibility for a colorimetric detector of the *relative* oxidative power of the constituents in organic solution. In addition to assessing chemical reactivity during a chemical reaction, this also provides a sensitive safety indicator, such as for peroxides in ether solvents. Figure S16 plots the relative Gibbs free energy for the 2-electron reactions of oxygen, nitrate, perchlorate, and hydrogen peroxide with the different halide species.[2] Note that we have only taken the simplest 2-electron reaction and not considered the subsequent oxidation reactions from the generated species. By using combinations of different $CsPbX_3$ halide P-NPs (X = I, Br, Cl), comparing the loss of fluorescence in the presence of different oxidative systems allows for the determination of relative oxidative strength via a simple colorimetric assay.

SUPPORTING FIGURES

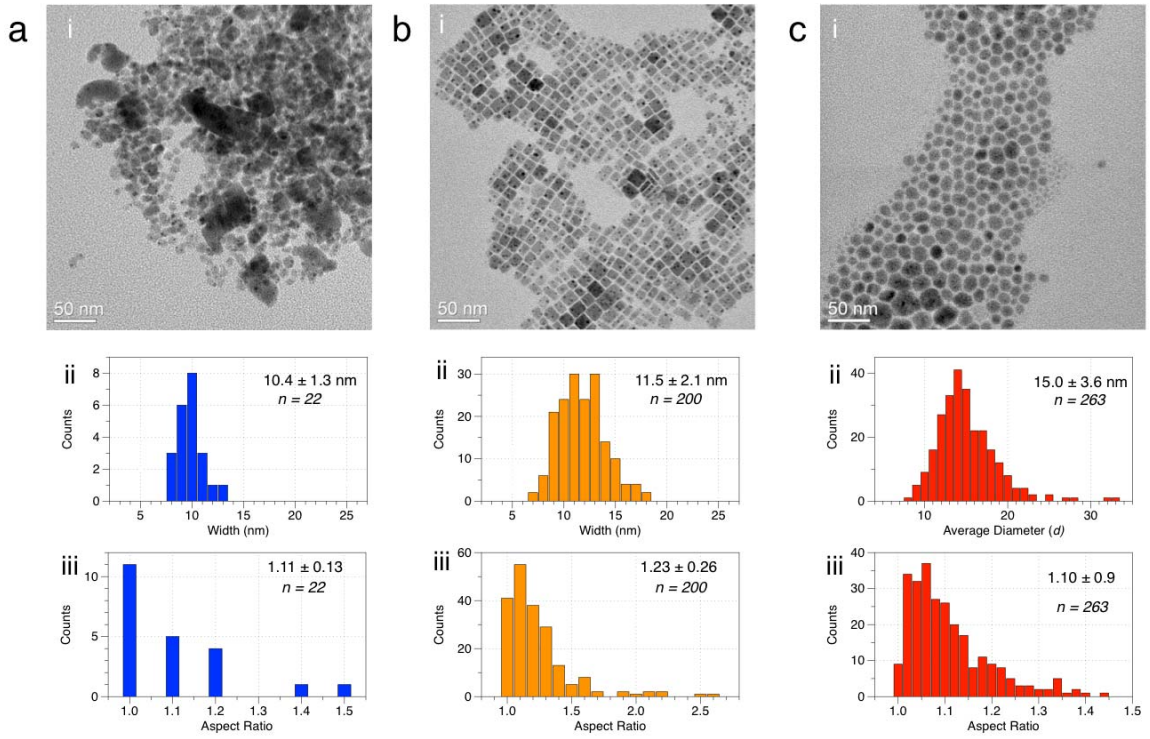

Figure S1: TEM images of $CsPbBr_3$ (a), $CsPbBr_{1.5}I_{1.5}$ (b) and $CsPbI_3$ (c) P-NPs with corresponding size (i) and aspect ratio (ii) statistics.

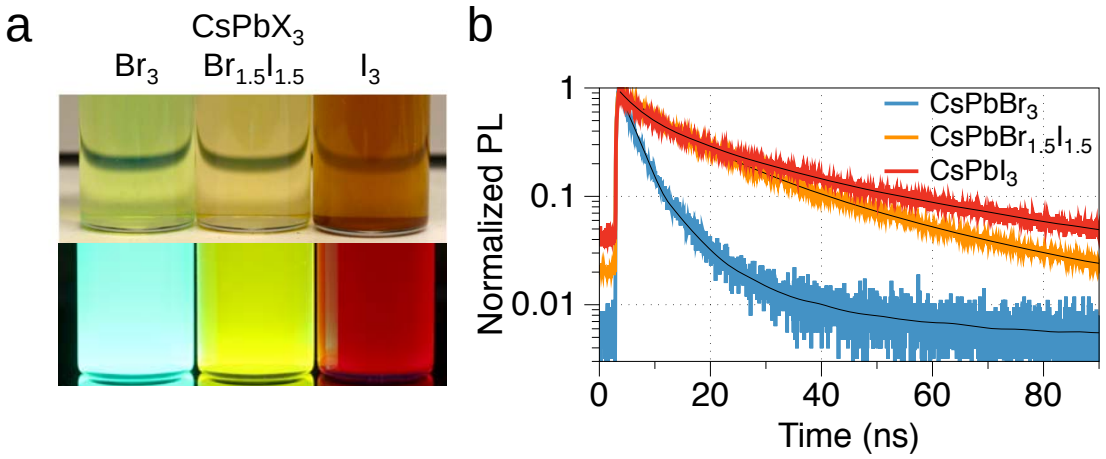

Figure S2: Optical images (a) of $CsPbX_3$ P-NPs in room light and under UV irradiation. PL decay curves (b) for $CsPbX_3$ P-NPs with $CsPbBr_3$, $CsPbBr_{1.5}I_{1.5}$ and $CsPbI_3$ having PL lifetimes of 5.4, 19, and 23 ns, respectively.

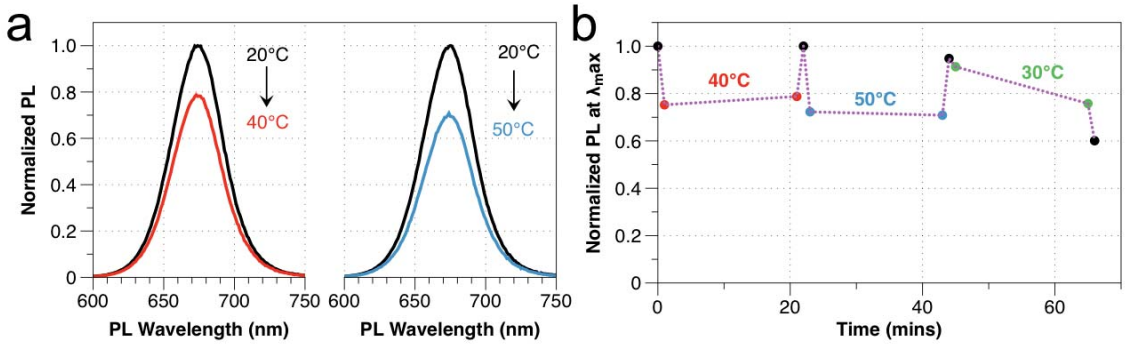

Figure S3: Spectra (a) and normalized intensity plots (b) of $CsPbI_3$ PL as a function of temperature. The P-NPs were found to be robust even at moderately high temperatures for a period of ~46 min, at which point the PL decreases.

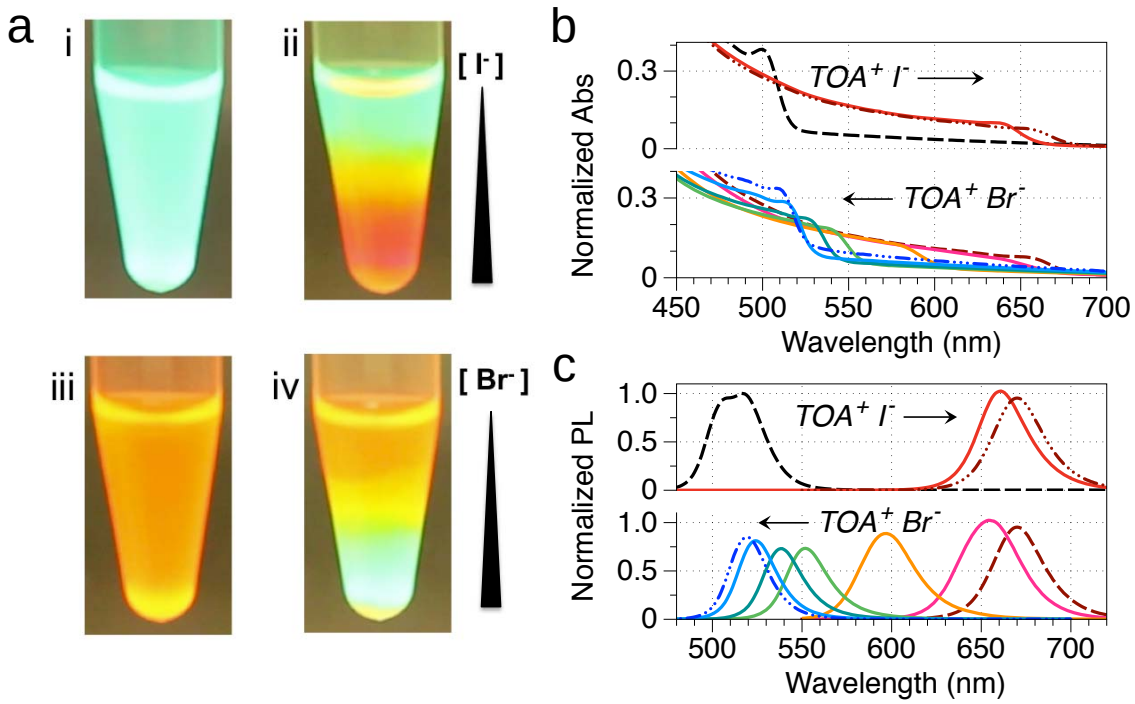

Figure S4: (a) Optical images of $CsPbBr_3$ P-NPs before (i) and after (ii) dropwise addition of TOAI dissolved in 1-butanol. Mixing the solution (iii) results in a uniform PL emission, but subsequent addition of twice the amount of TOABr results in the reverse gradient (iv). Representative absorbance (b) and PL (c) spectra are shown.

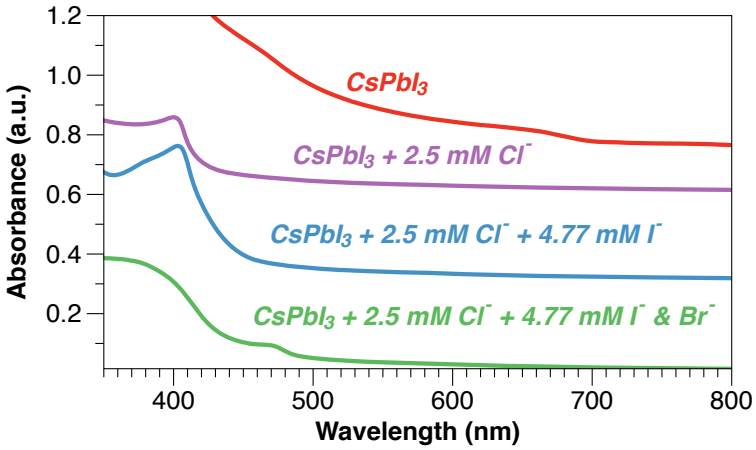

Figure S5: UV-Vis spectra of the sequential addition of $CsPbI_3$ P-NPs (red) with TOACl (purple), followed by TOAI (blue), and finally with TOABr (green), illustrating that transition of $CsPbI_3$ to $CsPbCl_3$ proceeds only in one direction, but can be reconverted to a mixture of $CsPbBr_xCl_y$.

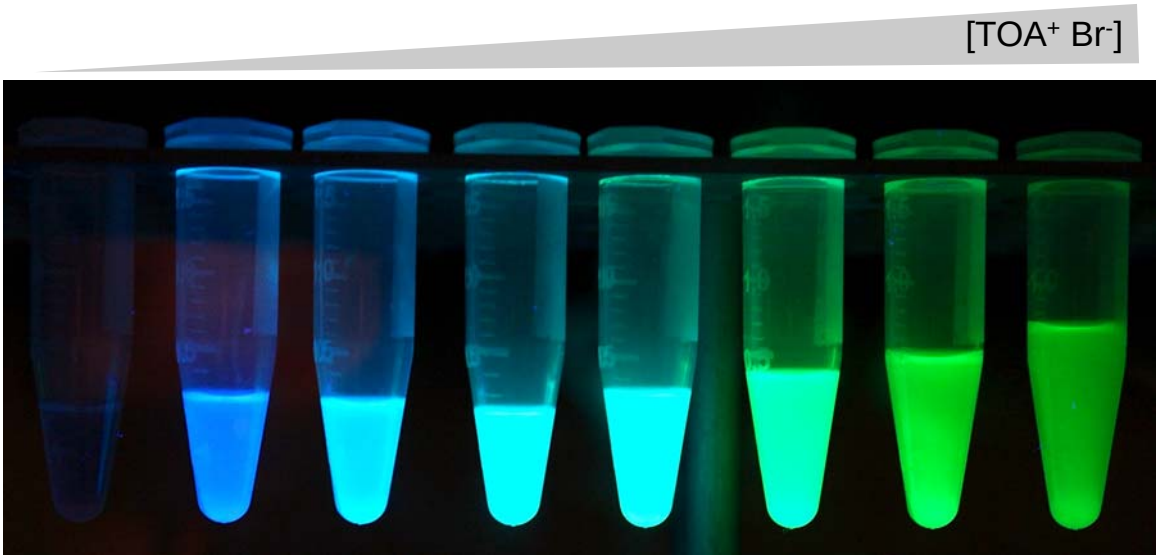

Figure S6: Image of the conversion of raw $CsPbCl_3$ NPs with TOABr in hexane from ultraviolet to green.

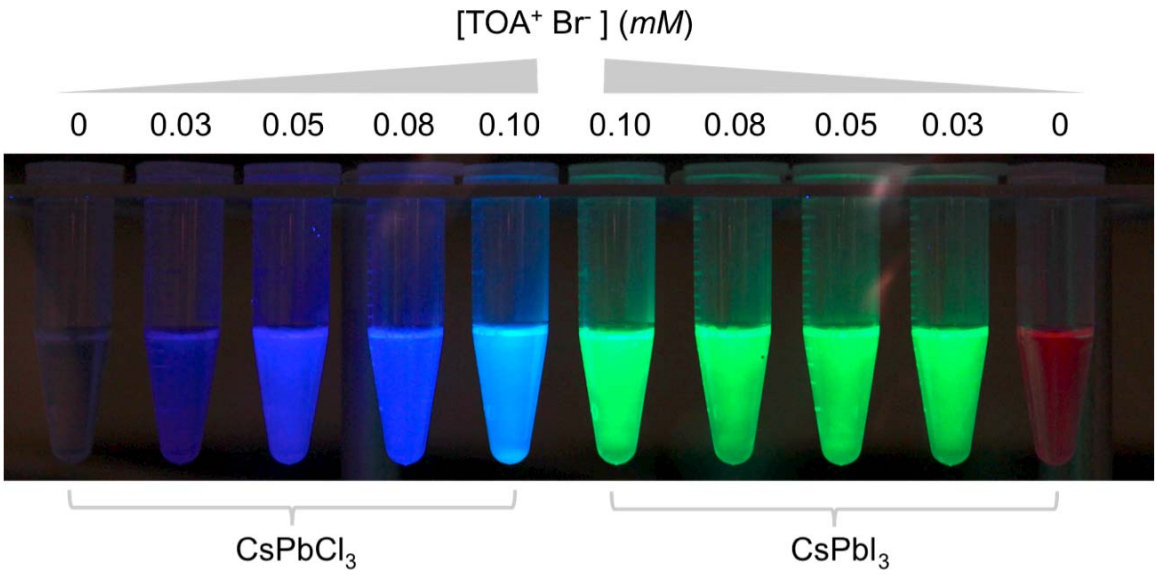

Figure S7: Image of the change in PL of $CsPbCl_3$ (left) and $CsPbI_3$ (right) diluted to the assay conditions reported in Figure 4 (~16 ug/mL) with increasing titration of TOABr in hexane, comparing the P-NP colorimetric response of increasing Br^- concentration anticipated in the 2-bromododecanoic acid reaction

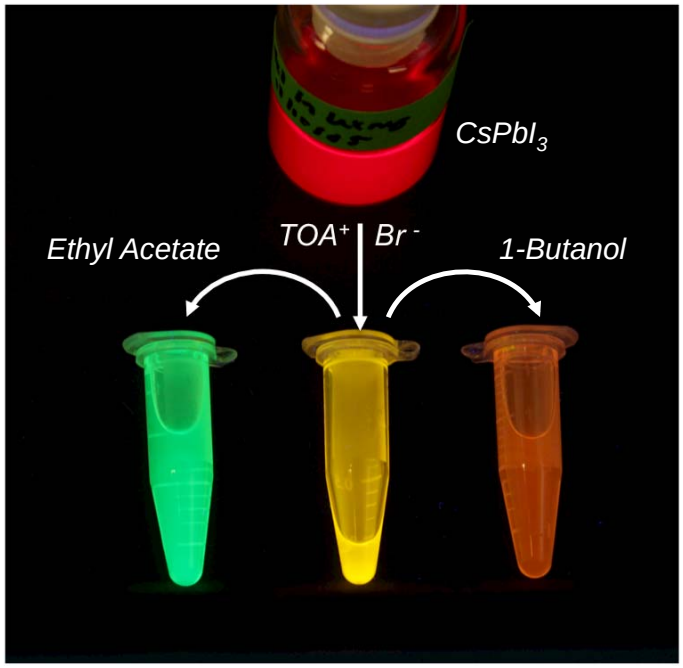

Figure S8: Image illustrating how conversion of raw $CsPbI_3$ P-NPs to a mixed $CsPbBr_xI_{3-x}$ P-NP with yellow emission, but dilution with ethyl acetate (ε_r~6.02) or 1-butanol (ε_r~17.51) leads to $CsPbBr_3$ or $CsPbI_3$ respectively due to changes to alklyammonium halide solubility.

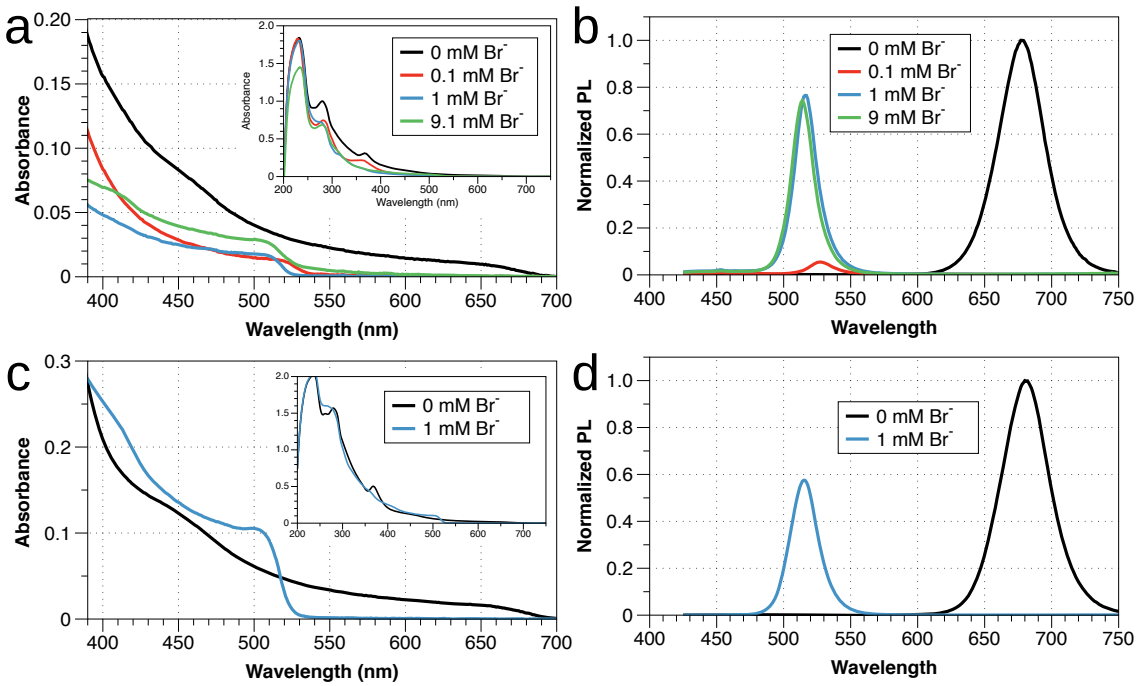

Figure S9: Comparison of spectral properties of $CsPbI_3$ P-NPs converted in 50-50 hexane/1-butanol (a and b) and in pure hexane (c and d) at different Br^- concentrations. Lower concentrations of Br- result in lowered PL of the final product relative to bulk additions, and the overall quantum yield is improved in a 50-50 mixture of butanol and hexane.

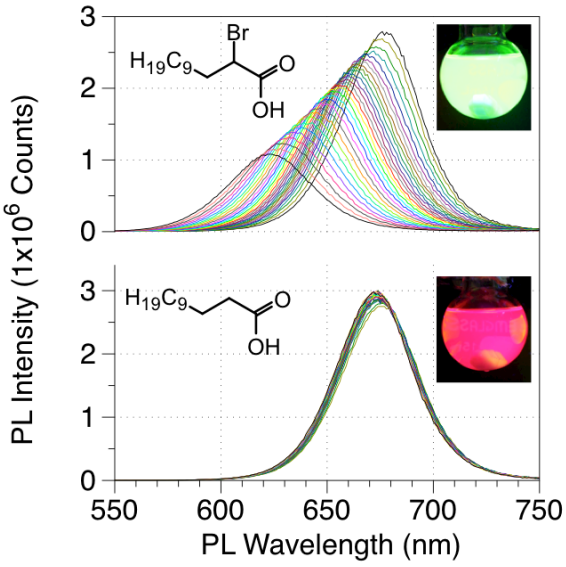

Figure S10: Comparison of the PL response of the P-NP colorimetric assay of the reaction involving 2-bromododecanoic acid (top) and dodecanoic acid (bottom) in the presence of octylamine, with only the halogenated compound showing reaction. Insets show optical images of the reactions in 15 mL reaction vessels after completion.

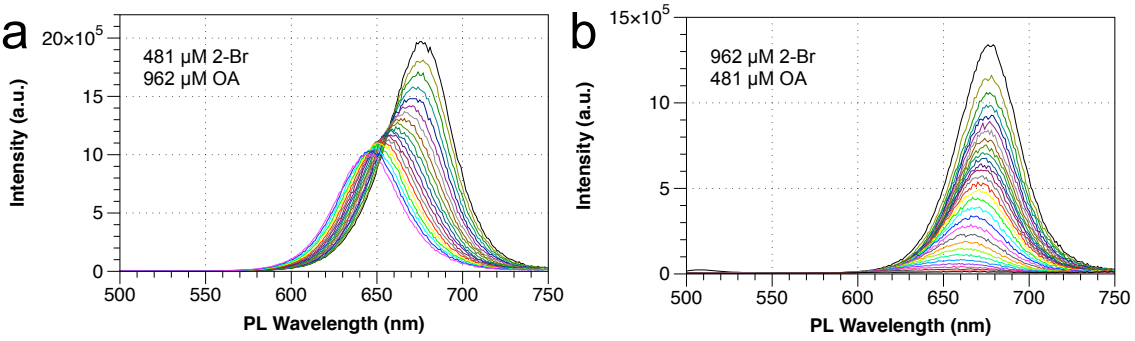

Figure S11: Comparison of the $CsPbI_3$ PL spectra in the presence of excess octylamine (a) and 2-bromododecanoic acid (b) as a function of time. Note that while doubling the amine does not dramatically affect the PL shift rate, doubling the 2-bromododecanoic acid results in fluorescence decay with only minor PL wavelength shift.

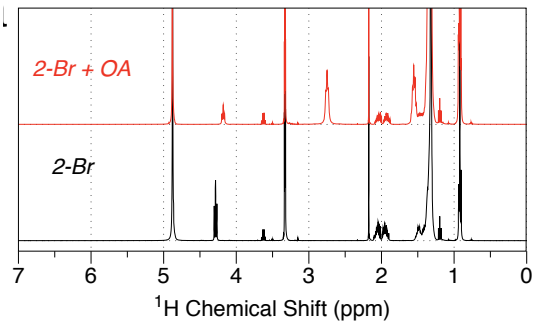

Figure S12: NMR spectra of the reactants in CD_3OD, revealing that the peak splitting at ~2 ppm for 2-Br in Figure 5a is due to ionization of the carboxyl group.

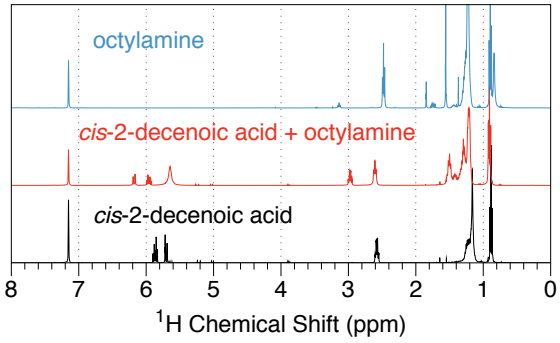

Figure S13: NMR spectra of purchased *cis*-2-decenoic acid alone (black) and in the presence of excess octylamine (red) in C_6D_6. The NMR spectra of octylamine alone (blue) is shown for reference.

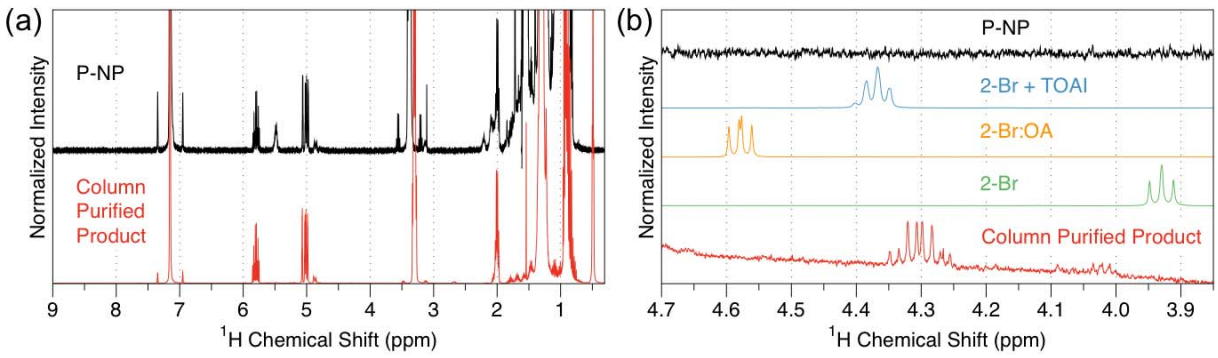

Figure S14: Comparison of the NMR spectra of the resulting product obtained from the reaction of 2-Br with the P-NP to the NMR of the P-NP alone (a) reveals substantial amounts of reagents used in P-NP synthesis remains after purification. Magnification of the 3.9-4.7 ppm region (b) reveals a shift of the α-H of 2-Br to ~4.3 ppm in the product (red), which is different from NMR of 2-Br (green) and 2-Br with equimolar OA (orange) alone. Comparison to the reaction of 2-Br with tetraoctylammonium iodide (TOAI) shows better correspondence indicative of a 2-I product.4. Note that the NMR spectrum of the P-NP (black) has no features in this chemical shift range.

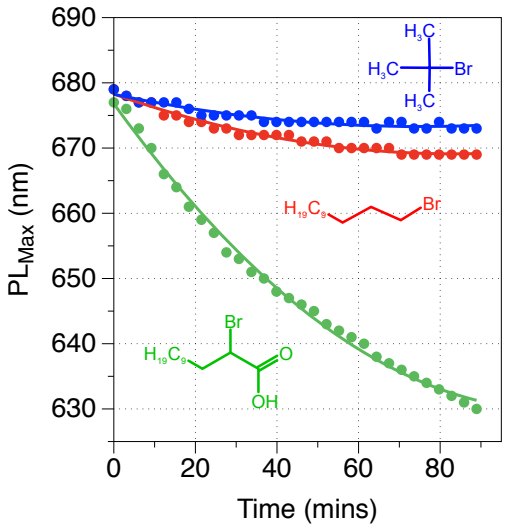

Figure S15: Kinetic monitoring of the chemical reaction involving octylamine and 2-bromododecanoic acid (green), 1-bromododecane (red), and *t*-butyl bromide at room temperature in the presence of $CsPbI_3$ NPs.

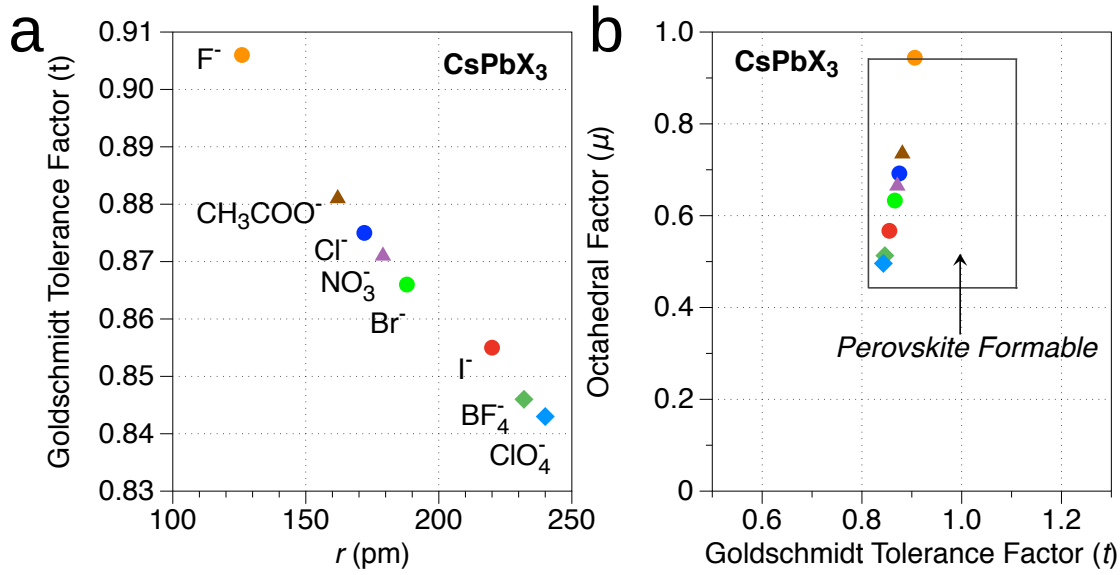

Figure S16: Comparison of the Goldshmidt tolerance factor (*t*) versus ionic radius (a) and the octahedral factor, μ, (b) for $CsPbX_3$ composed of different anions. Note that points within the box of (b) are considered to be perovskite formable.[6]

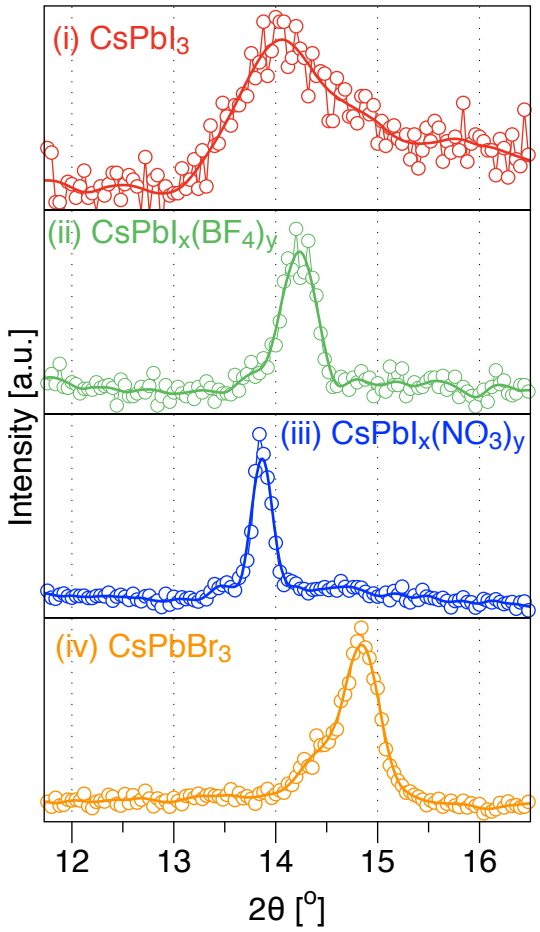

Figure S17: Powder XRD spectra of $CsPbI_3$ (i), $CsPbI_{3-x}(BF_4)_x$ (ii) $CsPbI_{3-x}(NO_3)_x$ (iii), and $CsPbBr_3$ (iv) compared along the <001> reflection of cubic perovskite lattice. The pronounced shifts indicate changes to the lattice parameter, likely due to partial anion exchange.

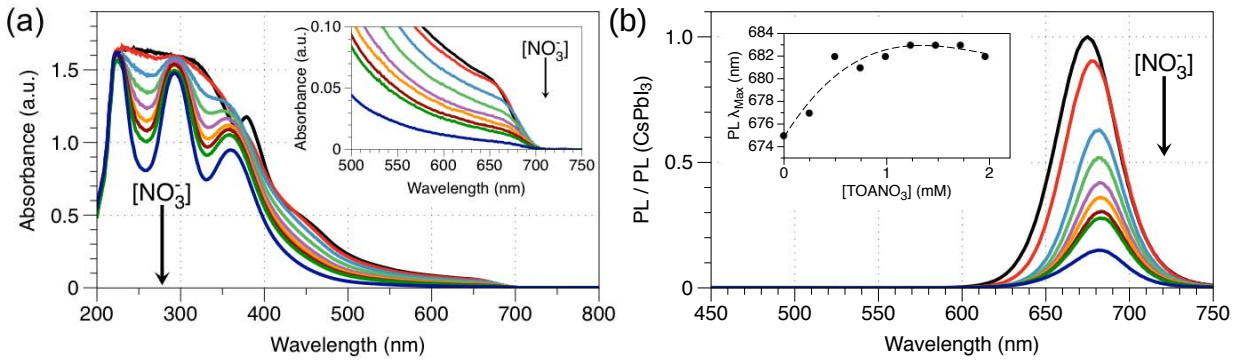

Figure S18: Absorbance (a) and photoluminescence (b) spectra of $CsPbI_3$ P-NPs after addition of tetraoctylammonium nitrate in increments of 0.24 mM NO_3^- from 0 to 1.9 mM. The inset in (a) magnifies the wavelength region of the first optical transition of the P-NPs, while the inset in (b) shows the corresponding shift of the emission maximum with increasing nitrate concentration. Shifting of the PL maximum is likely due to size selective oxidation. The distinct signatures with the large peak at ~300 nm are congruent with PbI_2,[9] and the peak at ~375 nm corresponding to I_3^-,[10] indicating that some oxidation is occurring with slow addition.

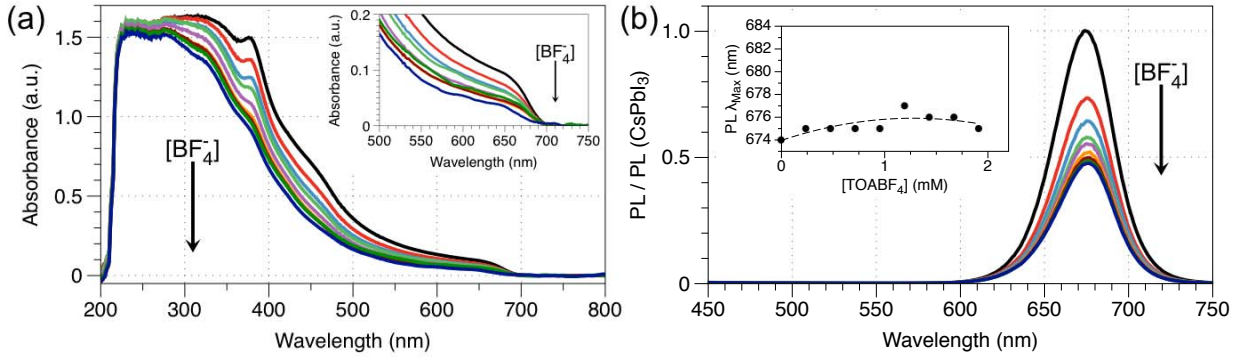

Figure S19: Absorbance (a) and photoluminescence (b) spectra of $CsPbI_3$ P-NPs after titration with 0.1M tetraoctylammonium tetrafluoroborate in increments of 0.24 mM NO_3^- from 0 to 1.9 mM. The inset in (a) magnifies the wavelength region of the first optical transition of the P-NPs, while the inset in (b) shows the corresponding shift of the emission maximum with increasing BF_4^- concentration.

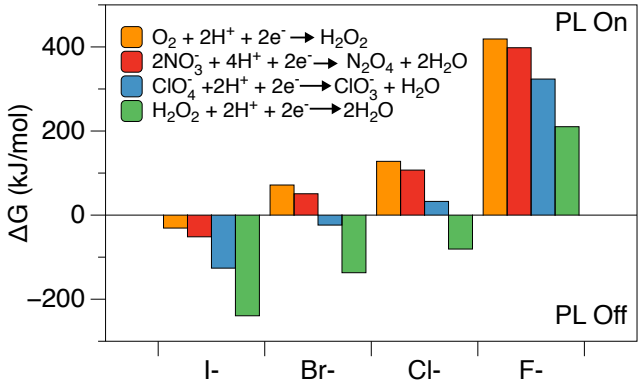

Figure S20: Plots of the free energy change (ΔG, kJ/mol) between the halides and selected oxidants based on the standard $2e^-$ reduction potentials.[2]

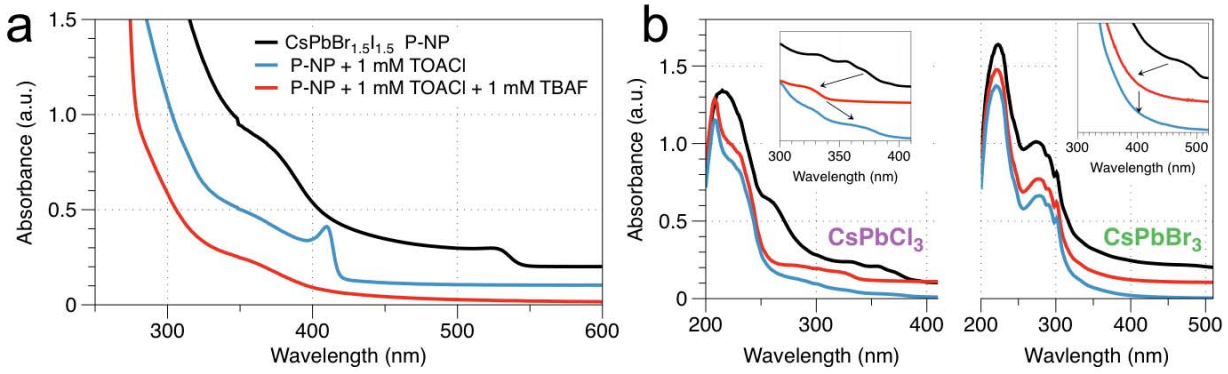

Figure S21: (a) Absorbance spectra of sequential additions of tetraoctylammonium chloride (TOACl) and tetrabutylammonium fluoride (TBAF) to $CsPbBr_{1.5}I_{1.5}$ NPs. (b) Absorbance spectra of unpurified $CsPbCl_3$ (left) and $CsPbBr_3$ (right) before (black), after the addition of 10 µL of 10 mM TBAF (red), and finally after 10 µL of 100 mM TOACl. Insets magnify the region around 300 nm to show reversible ion exchange in the case of $CsPbCl_3$ P-NPs but with no such shifts for $CsPbBr_3$.

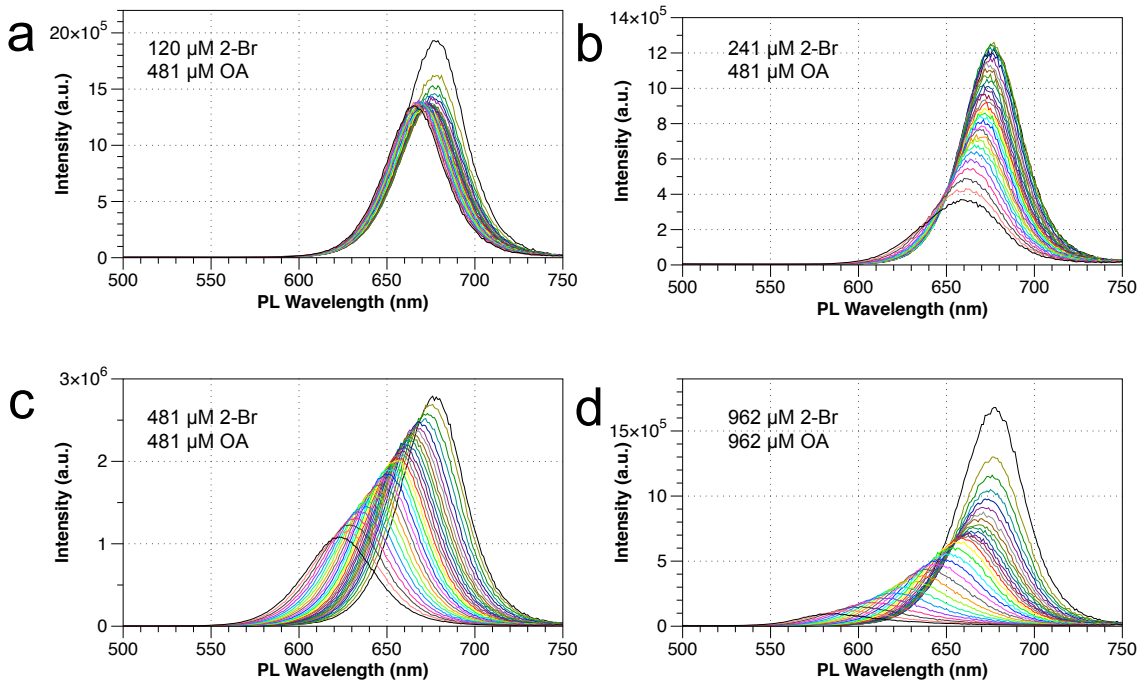

Figure S22: Comparison of the $CsPbI_3$ PL spectra in the presence of (a) 120 µM, (b) 241 µM, (c) 481 µM and (d) 962 µM with sufficient octylamine to undergo the elimination reaction as a function of time. The spectra shift from right to left with time corresponding with generation of Br^- in solution.

References

(1) Magde, D.; Wong, R.; Seybold, P. G. Fluorescence Quantum Yields and Their Relation to Lifetimes of Rhodamine 6G and Fluorescein in Nine Solvents: Improved Absolute Standards for Quantum Yields. *Photochem. Photobiol.* **2002**, *75*, 327–334.

(2) *CRC Handbook of Chemistry and Physics, 96th Edition*; Haynes, W. M., Ed.; CRC/Taylor & Francis, 2016.

(3) Ott, L.; Rijksen, C.; Ellinger, S.; Sievert, K.; Harloff, J.; Schulz, A. (Lonza Ltd.) Method for the preparation of tetraalkylammonium tetracyanidoborates. WO2014/29833 A1, 2014. Reaxys ID#: 37253354, Viewed 3/16/2016.

(4) Green, M. A.; Ho-Baillie, A.; Snaith, H. J. The Emergence of Perovskite Solar Cells. *Nat. Photonics* **2014**, *8*, 506–514.

(5) Jenkins, H. D. B.; Thakur, K. P. Reappraisal of Thermochemical Radii for Complex Ions. *J. Chem. Educ.* **1979**, *56*, 576.

(6) Li, C.; Lu, X.; Ding, W.; Feng, L.; Gao, Y.; Guo, Z. Formability of ABX_3 (X = F, Cl, Br, I) Halide Perovskites. *Acta Crystallogr. B* **2008**, *64*, 702–707.

(7) Shannon, R. D. Revised Effective Ionic Radii and Systematic Studies of Interatomic Distances in Halides and Chalcogenides. *Acta Crystallogr. Sect. A* **1976**, *32*, 751–767.

(8) Niu, G.; Guo, X.; Wang, L. Review of Recent Progress in Chemical Stability of Perovskite Solar Cells. *J Mater Chem A* **2015**, *3*, 8970–8980.

(9) Plekhanov, V. G. Lead Halides: Electronic Properties and Applications. *Prog. Mater. Sci.* **2004**, *49*, 787–886.

(10) Li, N.; Shi, L.; Wang, X.; Guo, F.; Yan, C. Experimental Study of Closed System in the Chlorine Dioxide-Iodide-Sulfuric Acid Reaction by UV-Vis Spectrophotometric Method. *Int. J. Anal. Chem.* **2011**, *2011*, 1–7.